Chapter 2

Novel Two-Dimensional Nanomaterial: High Aspect Ratio Titania Nanoflakes

Yang-Yao Lee

Additional information is available at the end of the chapter

http://dx.doi.org/10.5772/intechopen.73116

Abstract

A novel 2D nanomaterial, high aspect ratio TiO_2 nanoflakes were synthesized by a one-step method. Surface morphology and physical dimensions were characterized using Scanning Electron Microscopy (SEM), Laser Diffraction technology, and Transmission Electron Microscopy (TEM). Micro-sized flakes having a thickness approximately 40 nm were successfully synthesized by spreading a mixture of titanium alkoxide and hydrocarbon on the water surface. Relatively higher specific surface area (2–6 times) and less crystal defects enhanced photocatalytic activities of nanoflakes due to more surface reaction sites. By performing dye degradation under ultraviolet (UV) illumination, titania nanoflakes exhibited the higher photocatalytic efficiency over the commercial photocatalyst, Degussa P25. To the best of our knowledge, this is the first time to continuously synthesize low-dimensional nanomaterials in an efficient and cost effective manner. In practical water purification, traditional separation processes such as sedimentation or filtration could be utilized to easily extract the titania flakes from the treated water. Other applications such as anode material for lithium ion batteries and conducting paste in dye sensitized solar cells (DSSC) were also investigated. The cycling performance of Li-ion battery and energy conversion efficiency of DSSC were significantly improved.

Keywords: low-dimensional nanomaterials, titanium dioxide, nanoflakes, high aspect ratio, one-step synthesis

1. Introduction

Nanoscale functional materials, especially low-dimensional inorganic semiconductor materials have attracted great interest because of their size-dependent optical and electronic properties and potential applications in electronics and photonics. Because nanomaterials offer a high surface-to-volume ratio and short distance from the bulk material to the surface, the

preparations are vivid [1]. Researchers have been focused on the morphology control, such as synthesis of nanotubes [2], nanowires [3, 4], nanoribbons [5], diskettes [6], nanobelts, nanosaws, nanowalls, nanomultipods, nanorings, nanocages, nanohelixes, nanopropellers, and many others [7–9]. While one-dimensional nanomaterials such as nanowires and nanorods have been extensively studied, 2D nanostructured materials have attracted relatively less attention. However, 2D nanomaterials show strong potential as chemical and biological sensors, nanoelectronic devices, and catalysts with high surface areas and large pore volumes. Many small band gap materials such as ZnO, ZnS, and Bi_2WO_6 with flake-like or plate-like morphologies have been already synthesized successfully [10–12]. For example, Ye et al. synthesized thinner ZnO nanoplates by restricting the crystal growth along (0001) plane with complexation between Zn^{2+} and citrate ions. The 50 nm thick hexagonal nanoplates with uniform 1 μm diameter presented the highest photocatalytic activity over other morphologies including nanorods, microrods, and dumbell-shaped microrods [13]. Liu et al. developed a combustion CVD method to deposit 50 nm to 1 μm thick ZnO flakes on Si substrate for ethanol vapor sensing [14]. Duan et al. developed an integrated autoclaving and pyrolysis process to obtain porous hexagonal ZnO micro-flakes [15]. Amano et al. autoclaved the mixture of bismuth nitrate and sodium tungstate to precipitate thin Bi_2WO_6 crystalline platelets (20–25 nm) with shifted absorption edge to the longer wavelength at 440 nm. The tungstate nanoplates completely oxidize gaseous acetaldehyde under visible light illumination resulting from slow recombination and a long lifetime of generated carriers in the time-resolved infrared absorption spectra [11]. Lanthanum titanate ($La_2Ti_2O_7$) flakes were prepared by the reaction of titanium sulfate and lanthanum nitrate under the hydrothermal condition [16]. The thin lanthanum titanate flakes demonstrated significantly higher photoactivity to produce water splitting H_2 from water under UV irradiation over conventional solid-state reaction material due to higher surface area and light absorption. Highly porous CoOOH flakes were prepared by the deposition of layered cobalt acetate hydroxide solution on a nickel foil in 1.0 M KOH solution. The cyclic voltammetry (CV) measurements indicated high rate capacitance with good cycle ability of CoOOH flakes [17]. A novel pigment derived from silica flakes coated with titania from a web coating process were developed in a range of 50–1000 nm thickness [18]. The special color variation effect is achieved by the combination of silica flakes and titania coating resulting in strong light interference and angle-dependent behaviors. Nanosheets with a spacing of 0.6 nm were precipitated on a glass substrate from a SiO_2-TiO_2 gel solution under vibration in a 90°C hot water bath [19]. The good hydrophilicity and antifogging capability without any light exposure for 2000 h received from the hydrated nanosheets with unique physicochemical properties such as roughness and surface chemistry. Although the above materials possess unique properties on optical, gas sensing, electrochemical, and cleaning applications, the relatively expensive precursors or processes hinder practical applications.

Titanium dioxide is a versatile and low cost material for many industrial applications; many scientific works have been focused on particle size control down to the order of tens of nanometers. Nanostructured titanium dioxide were continuously developed in the field of environmental purification, solar energy conversion, pigment, optics, gas sensing, and energy storage [20–22]. However, using TiO_2 nanoparticles for water treatment is limited because of

the difficulty of separation from purified water. Besides isotropic nanoparticles, anisotropic nanostructures including nanotubes, nanowires, nanorods, nanofibers, and nanosheets have been successfully synthesized [3, 23–26].

2. High aspect ratio titania nanoflakes

2.1. Syntheses of 2D titania nanomaterials

The most common shape of the fine titanium dioxide particles is spherical in many syntheses and applications. Thin films or fibers have been fabricated by being supported on a substrate or in the interstices in some three-dimension network [27, 28]. Sasaki fabricated thin titania flakes through exfoliation of a layered titanate precursor [25]. Although the specific surface area of the flakes is about 110 m^2/g, the photocatalytic activity is still less than commercial product, Degussa P25 (49 m^2/g). The freeze-dried nanosheets were also adopted as the anode material in a liquid electrolyte lithium ion battery [29]. The promising electrochemical performance of titania nanosheets were exploring in the charge-discharge characterizations as discharging with smaller slope and lower average voltage than titanium dioxide and lithium titanate. Li et al. in 2007 synthesized Brookite phase titania nanoplates by using titanium trichloride ($TiCl_3$) precursor through hydrothermal processes [30]. Under the same surface area of loaded TiO_2, the brookite nanoplates exhibit the highest efficiency in the beaching of methyl orange solution under UV irradiation. The lamellar titania were synthesized within the lamellar micelle of non-ionic surfactant in cyclohexane [31]. The resembling nanostructures consisted of 40 nm titania flakes with flat, homogenous surface and low defects. Wu et al. utilized the micro-arc oxidation process associated with alkali treatment at pure titanium substrate to develop titania flakes [32]. However, most synthesis methods for these types of particles require multiple, complicated procedures and are typically nonconductive to be scaled up manufacturing as yields are typically milligram or less quantities of material. Examples include template, chemical vapor deposition, hydrothermal, electrochemical anodization, etc. [33–36].

2.2. One-step synthesis of titania nanoflakes

Anatase powders with sizes ranging from 5 to 165 nm were employed various synthesis methods. Regardless of fabrication processes, the optimum particle size range of 25–40 nm within all photocatalytic experiments processes were suggested by Almquist and Biswas [37]. The optimum photocatalysis is a function of competing mechanisms such as light absorption and scattering efficiency of the particles, as well as electron–hole pair combination and interfacial charge transfer. Therefore, we believe a one-step synthesis for titania nanomaterials with at least 1D close to the optimum size of photocatalyst will be a revolution of the titania photocatalyst fabrication. The one-step synthesis is spreading an oil phase consisting of titanium tetraisopropoxide and a low surface tension hydrocarbon at the surface of water to produce micrometer sized titania flakes having a thickness around 40 nm [38, 39]. Moreover, the thickness of nanoflakes could be tuned by changing the volume ratio of titania precursor and hydrocarbon. For instance, 40 nm titania flakes were successfully synthesized using a ratio of

1:8 of titania tetraisopropoxide to hydrocarbon. The reactions of forming TiO_2 in this research could be represented as follows:

$$Ti\left(O\,C_3\,H_7\right)_4 + 4\,H_2\,O \;\rightarrow\; Ti\,(OH) + 4\,C_3\,H_7\,OH\ldots(hydrolysis) \tag{1}$$

$$Ti\,(OH)_4 \;\rightarrow\; Ti\,O_2 + 2\,H_2\,O\ldots(condensation) \tag{2}$$

The resulting slurry was washed with Nanopure water and isoproponal thoroughly to remove impurities. Dried and well dispersed particles were collected by the supercritical fluid drying process [40]. The following heat treatment for phase transformation was conducted at 400°C. This synthesis has high potential to manufacture gram to kilogram quantities of nanomaterials. Scanning electron microscopy (SEM), laser diffraction analysis, X-ray diffraction (XRD), transmission electron microscopy (TEM), and physisorption techniques were used to further characterize these titania nanoflakes.

2.3. Characterization of titania nanoflakes

The surface morphology of synthesized titania nanoflakes was investigated using SEM images. The images revealed the major diameter was within the order of 10–20 μm and the thickness was approximately 40 nm (**Figure 1**). Agglomerations or aggregations were not observed under SEM review when comparing the received samples with and without calcination. Moreover, the thickness of calcined flakes did not changed by the heat treatment. Both the uncalcined and calcined flakes were transparent under the SEM. The surface morphology of titania nanoflakes were similar to exfoliated nanosheets and micro-arc oxidized flakes on titanium substrate (**Figure 2**) [25, 32]. Light scattering technology such as laser diffraction were also used to quantified the particle size distributions of synthesized and calcined flakes. Theoretically, laser diffraction analysis alone is not designed for characterizing size distribution of anisotropic particles. To have a better understanding of the particle morphology, conjunction with electron microscopic method is necessary. Comparable data of major dimension were obtained by two methods. The statistics data of particle size distribution by volume were shown in **Table 1**. The synthesized material has wide size distribution spanning from 1 to 100 μm with a D_{50} of 20.8 and 19.0 μm for the synthesized and calcined flakes respectively (**Figure 3**). Some larger flakes may crack or break during the re-crystallization and dehydration in terms of the volume distributions. The average aspect ratio of the flakes is 1:500 resulting from the calculation which divided mean size by thickness (**Table 1**). Powder X-Ray Diffraction (XRD) monitored the crystalline structure changes of the titania flakes during the heat treatment (**Figure 4**). The synthesized flakes show broadening and weak peaks which suggests the mixture of amorphous material with a presence of the anatase phase. Pure anatase phase [JCPDS: 21-1272] which is the most photoactive structure were identified by XRD with the seven diffraction peaks in the heat treated flakes [41–43]. No other common phase such as rutile were observed by XRD. Complete phase conversion of amorphous titania was confirmed by comparing the intensity characteristics peaks between calcined flakes and the commercial pure anatase standard materials. The average crystal grain size can be calculated by the Scherer equation:

$$d = \frac{k\lambda}{B\cos\theta_B} \tag{3}$$

Where d is the calculated grain size, λ is the wavelength of X-ray (Cu Kα 1.54 Å), β is the full-width at half-maximum intensity, and θ_B is the half of the diffraction peak angle. The grain size was determined to be 4 and 9 nm for synthesized and calcined flakes respectively (**Table 2**). High resolution transmission electron microscopy (HR-TEM) images revealed circular crystalline platelets of about 5–8 nm in diameter (**Figure 5**). The interference lattice fringes with separation distance of 0.35 nm corresponded to the interplanar spacing of the (101) planes for anatase [44]. The concentric diffraction rings in the select area diffraction mode indicated random orientation of individual grains over the both flakes which is consistent with the anatase (101), (004), (200), (105) for circles 1–4 respectively (the insets of **Figure 5**). On closer inspection, synthesized samples contained an amorphous layer can be seen surrounding the smaller circular crystallites (**Figure 5a**). After calcination, calcined samples developed some pores due to local rearrangement and growth of crystal grains (**Figure 5b**). Consequently, polycrystalline fine grains of anatase populated throughout the whole calcined flakes. The nitrogen absorption isotherms in conjunction with the Brunauer-Emmett-Teller (BET) model was used

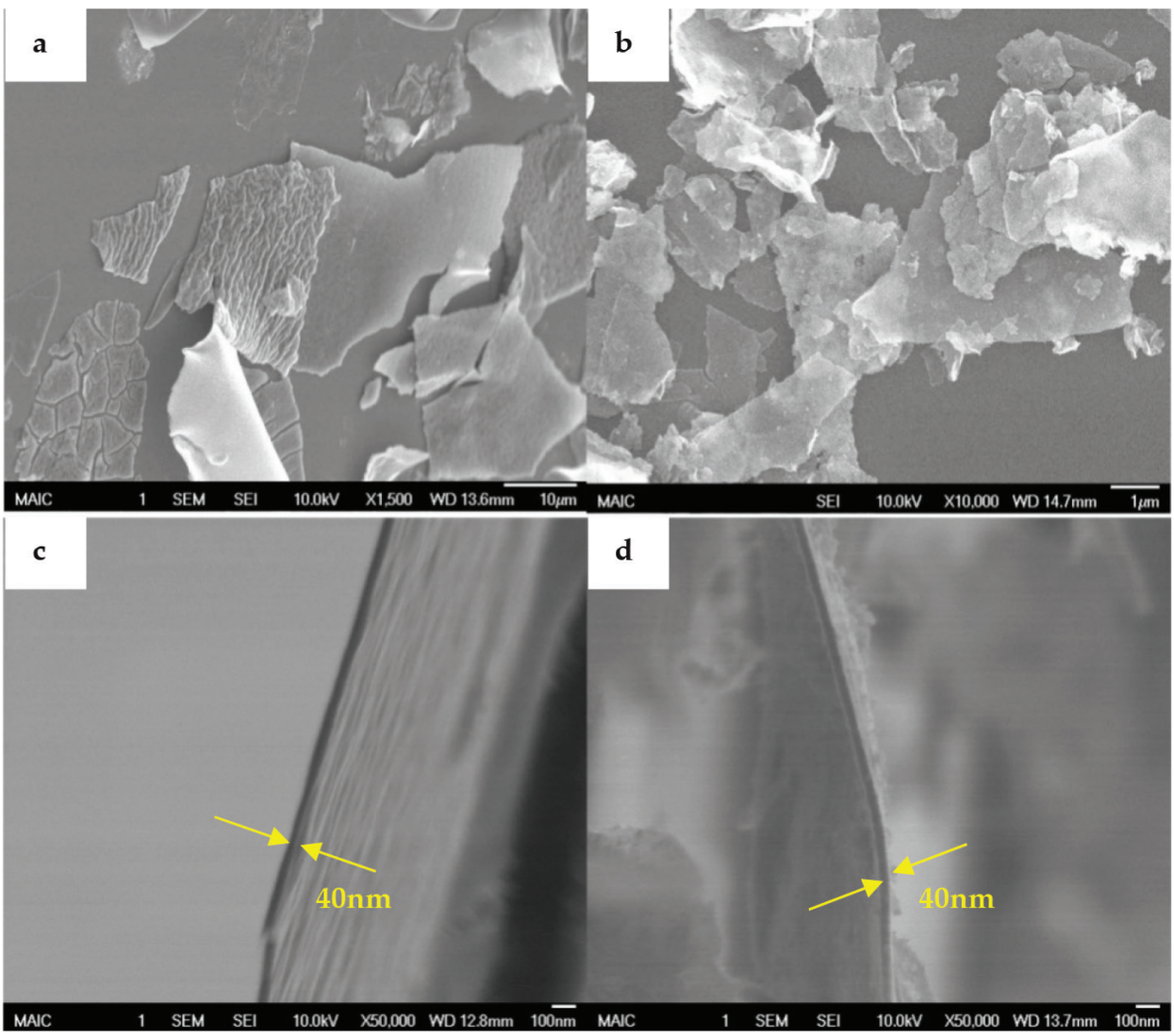

Figure 1. SEM images of titania nanoflakes: (a) synthesized samples (b) calcined samples (c, d) edge views of A and B respectively. Images were obtained without conducting coating.

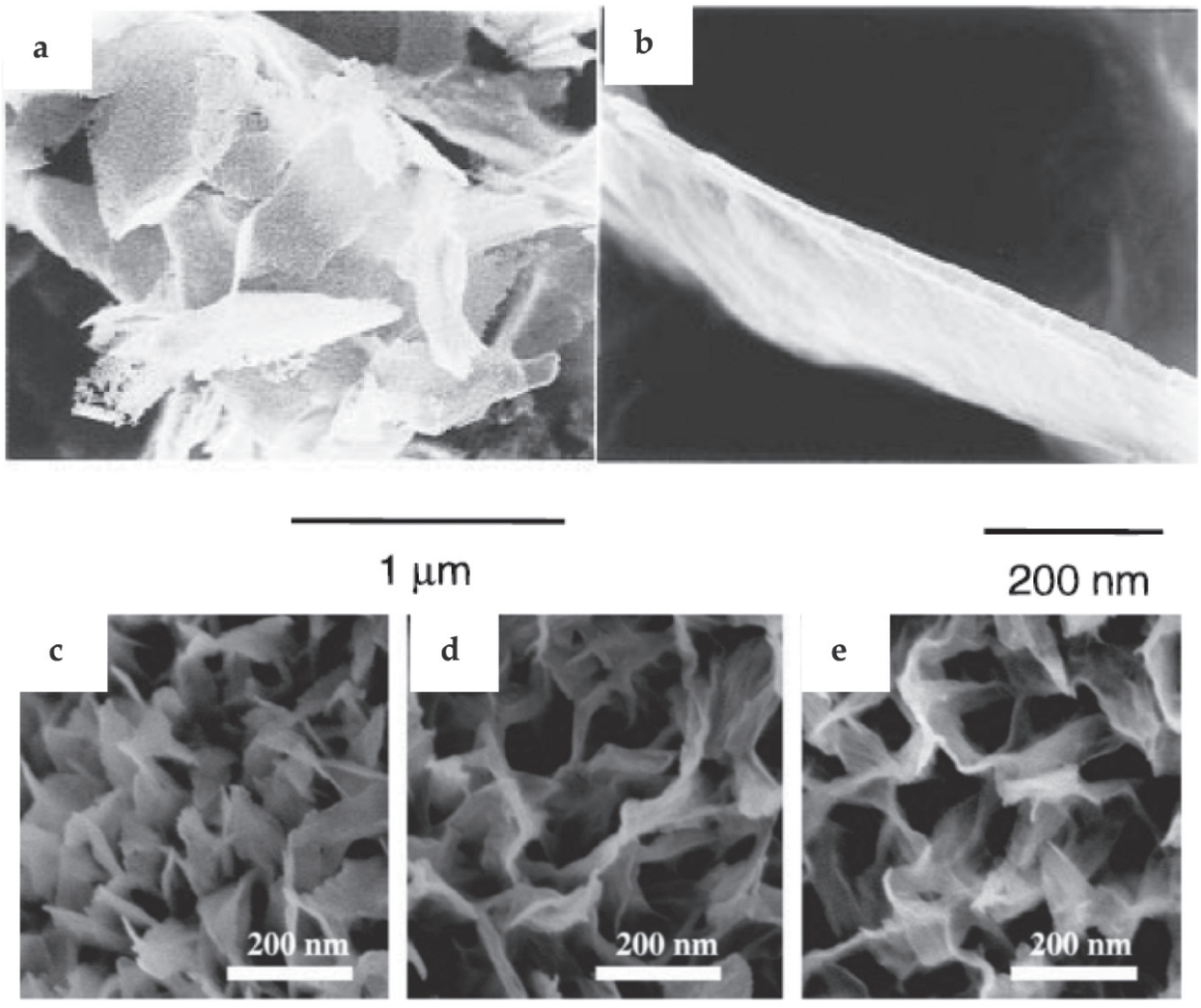

Figure 2. Literature SEM images of titania flakes: (a) heated at 700°C (b) edge view [25] (c, d, e) micro-arc oxidation flakes in alkaline solution of 1.25 M, 2.5 M, and 5.0 M respectively [32].

to estimated the specific surface area of synthesized and calcined titania nanoflakes. Higher specific surface area usually leads to higher photoactivity from larger amount of adsorbed organic molecules at surface sites which enhance the reaction rate. However, it is usually simultaneously with higher amounts of crystal defects favoring recombination of charge carriers leading to lower photoactivity. Compared to a commercial photocatalyst, Degussa P25 [45], 2–6 times higher surface area were obtained by titania nanoflakes (**Table 3**). The photocatalytic activity of these flakes was investigated by performing dye degradation experiments under ultraviolet activation.

Sample	D_{10} (μm)	D_{50} (μm)	D_{90} (μm)	Mean (μm)	Standard deviation (μm)
Synthesized flakes	5.2	20.8	81.6	39.1	58.9
Calcined flakes	5.1	19.0	51.8	24.7	20.9

Table 1. Particle diameter statistics for synthesized and calcined titania flakes under investigation.

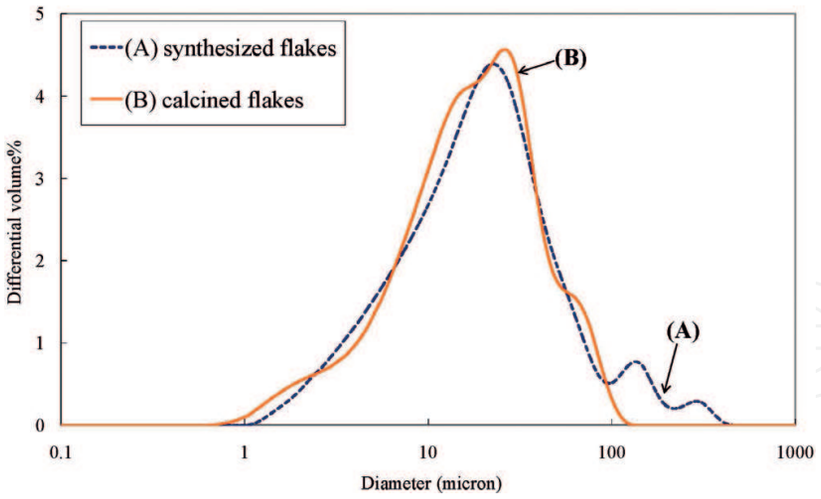

Figure 3. Volume based particle size distribution for synthesized and calcined titania flakes.

2.4. Applications of titania nanoflakes

2.4.1. Photocatalysis of titania nanoflakes

Using TiO_2 nanoparticles for water treatment is limited in practical application since it is very difficult to remove these ultrafine particles due to very small mass. Therefore, the conventional separation methods such as centrifuging, filtration, and sedimentation are difficult and expensive to implement. In addition, the efficiency of photodegradation by using nanoparticles is not very high because of the poor accessibility of the organic pollutants to catalyst surface caused by the agglomeration of particles [46]. Synthesizing larger flake-like titania with nanosized thickness will alleviate this problem. These titania flakes can be easily separated from the treated water by simply filtration or sedimentation. Because the flakes are nano thin, superior photocatalytic properties are retained due to high surface to volume ratios and short diffusion paths, which are favorable for the migration of electrons and holes. This reduces the

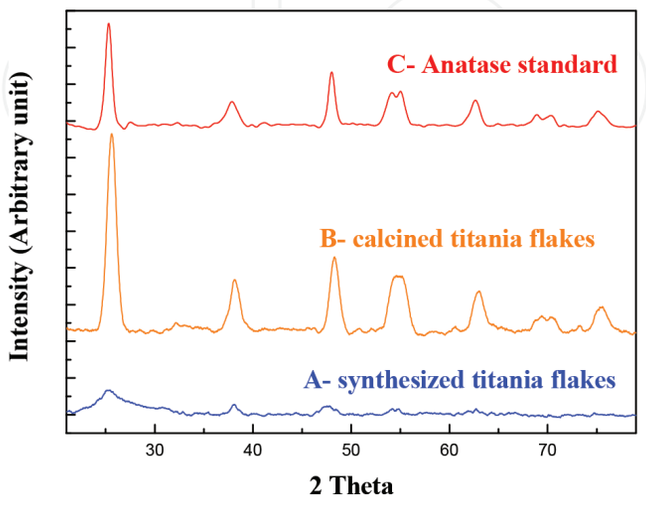

Figure 4. XRD patterns of synthesized and calcined titania nanoflakes.

Sample	θ_B (degree)	d (nm)
Synthesized flakes	25.91	4.1
Calcined flakes	25.35	8.7

Table 2. Grain size calculation by the Scherer equation for both nanoflakes.

probability of the recombination of photogenerated electrons and holes. At the same time, the common agglomeration problem caused by nanoparticles can also be mitigated and therefore maintain the advantages of micro and nanostructure. The photocatalytic efficiency of titania nanoflakes were investigated by UV-visible spectroscopy and degradation of methylene blue under UV irradiation. The typical light absorption of the semiconductor materials such as titania showed the sharp decrease in the diffuse reflectance in the UV region (**Figure 6**). Calcined sample demonstrated a blue shift of the onset of reflectance. In semiconductor physics, the general relation between the absorption coefficient and the band gap energy is given by

$$(\alpha h\nu)^m = h\nu - E_g \tag{4}$$

Where m is an index depending on the nature of the electron transitions, α is the absorption coefficient, h is the Planck constant, ν is the frequency of electromagnetic radiation, and E is band gap energy of the semiconductor. The optical absorption energy of both nanoflakes were determined via extrapolation of $(\alpha h\nu)^2$ versus hν plot (**Figure 6b**). The quantum confinement effect of higher crystallinity after calcinations and thin flaky morphology could result in an increase in band gap from 3.25 to 3.33 eV, i.e. a blue shift [47]. **Figure 6** compares the photocatalytic activity of P25, synthesized and calcined titania nanoflakes by removing the

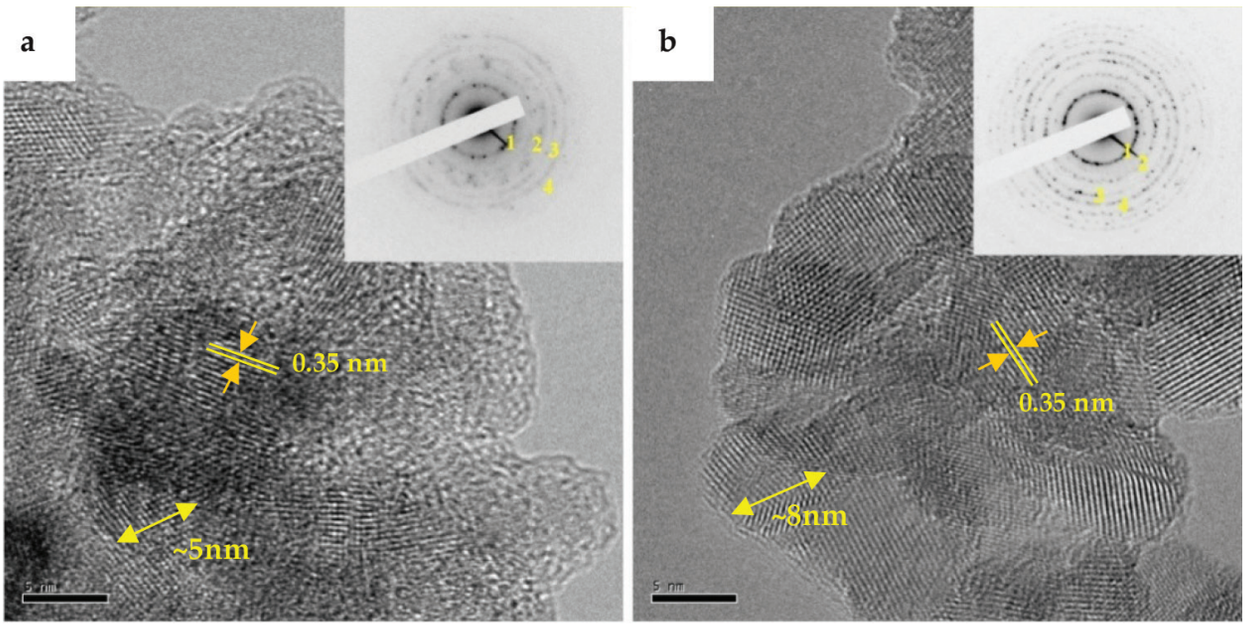

Figure 5. HR-TEM images of titania nanoflakes (the SAD pattern as inset) (a) synthesized samples (b) calcined samples the diffraction rings are indexed as (1) 101 (2) 004 (3) 200 (4) 105 for anatase.

Sample	Specific surface area (m^2/g)	Specific pore volume (cm^3/g)
Synthesized nanoflakes	323	–
Calcined nanoflakes	110	0.342

Table 3. Physisorption measurements of P25, synthesized and calcined titania nanoflakes.

methylene blue form water under UV light illumination. For comparison, Degussa P25 was used as a reference material. Among all tested samples, calcined flakes exhibited the highest photocatalytic efficiency on the dye degradation. A first order rate reaction was observed which suggested dye concentration is the limiting factor (**Figure 7**). In contrast, significant enhancement was observed when agitation was added to the system by continuously introducing air bubbles (**Figure 7b**). A pseudo first order reaction was obtained by adding turbulence resulted in much higher efficiency especially for the flake systems. The oxygen depletion during the photocatalysis process could be one possible explanation of these differences. The flake samples have much higher surface area than P25 and consisted of very small nanocrystallites which imply a large amount of defects (grain boundaries) from the results of XRD and TEM. Fast recombination of photoassisted electron and hole pairs preferentially occurs at these local defect sites and dominates the reaction. Without supplying oxygen to the system, the photocatalytic performance is therefore not proportional to surface area. However, dissolved oxygen may form superoxide radicals as the electron acceptor when applying oxygen to the system [48]. More importantly, eliminating excited conduction band electron would help to suppress the rate limiting step, fast recombination, and result in higher efficiency.

2.4.2. Other applications: Li-ion battery and DSSC

Anatase titanium dioxide is a promising negative electrode material for Li-ion batteries. However, the low intrinsic electrical conductivity and poor cycling performance have limited its application. Among all anatase titania samples, the calcined titania flakes performed higher rate capability, larger reversible capacity, and longer cycling stability [49]. The better

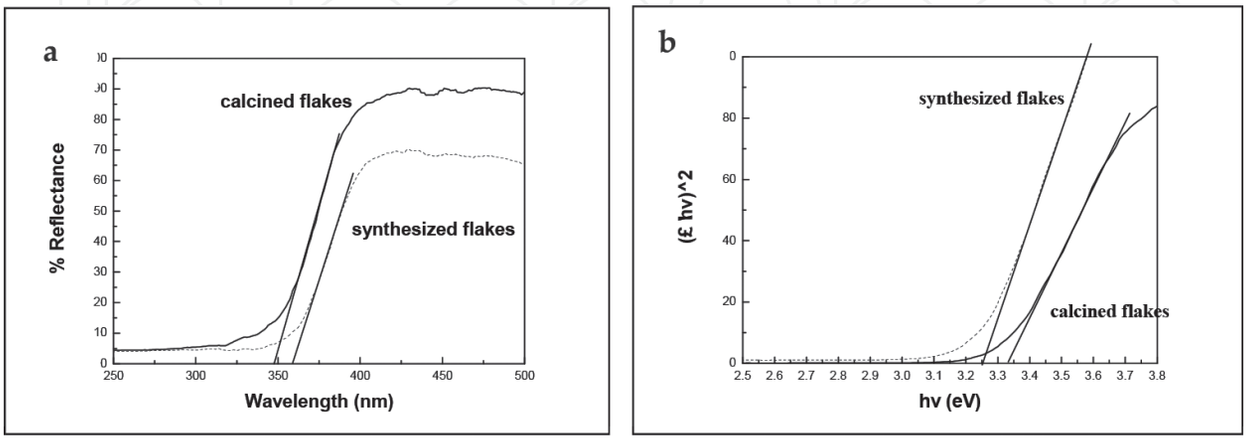

Figure 6. (a) Diffuse reflectance spectra and (b) the dependence of $(\alpha h\nu)^2$ on the photon energy for synthesized and calcined titania flakes.

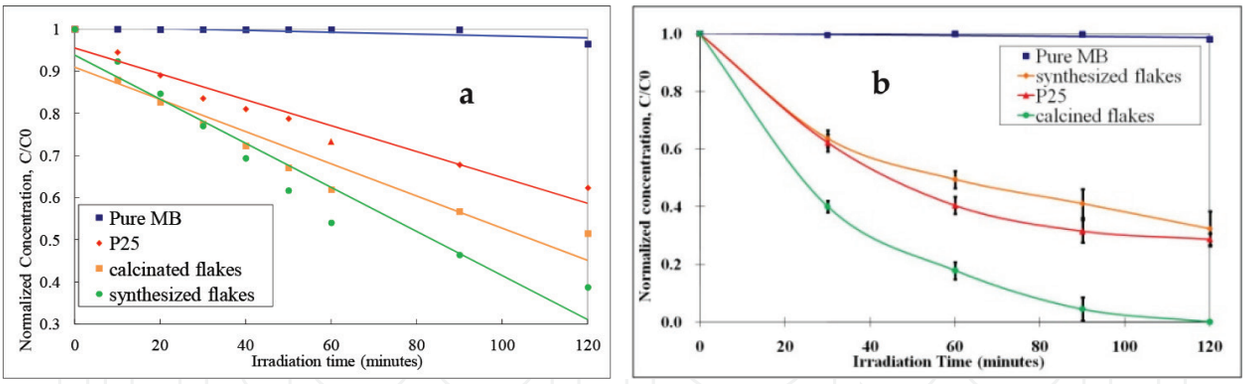

Figure 7. Photocatalytic decomposition of methylene blue by using synthesized and calcined flakes (a) without bubbling treatment (b) with bubbling treatment.

charge/discharge and rate capabilities resulted from the higher specific surface area of the flakes which leads to faster transportation between Li-ion and electron within the matrix of titania lattice (**Figure 8a**). Besides, the porous morphology of the calcined flakes provided extra space for the volume change during cycling and therefore significantly improved the cycling performance (**Figure 8b**).

Using the same deposition method to assemble the DSSC, integrally and closely bonded films resulted from better particle dispersion of titania flakes (**Figure 9**). In contrast, discontinuity of P25 nanoparticle layers were observed after the evaporation and sintering processes [50]. Improved energy conversion efficiency of DSSC could be attributed to two features of titania flakes: (1) Stronger adsorption of visible dyes from high specific surface area (2) Micron scale in two dimensions lead to stronger light scattering of visible light spectrum. The important IV characteristics of DSSC such as short-circuit current density (I_{sc}) and open-circuit voltage (V_{oc}) were found to be related to the thickness of the TiO_2 photoelectrodes. According to the calculations, calcined titania flakes demonstrated 5 times higher efficiency over the P25 photoelectrodes under the same thickness basis (7.4% vs. 1.2%) (**Figure 10**).

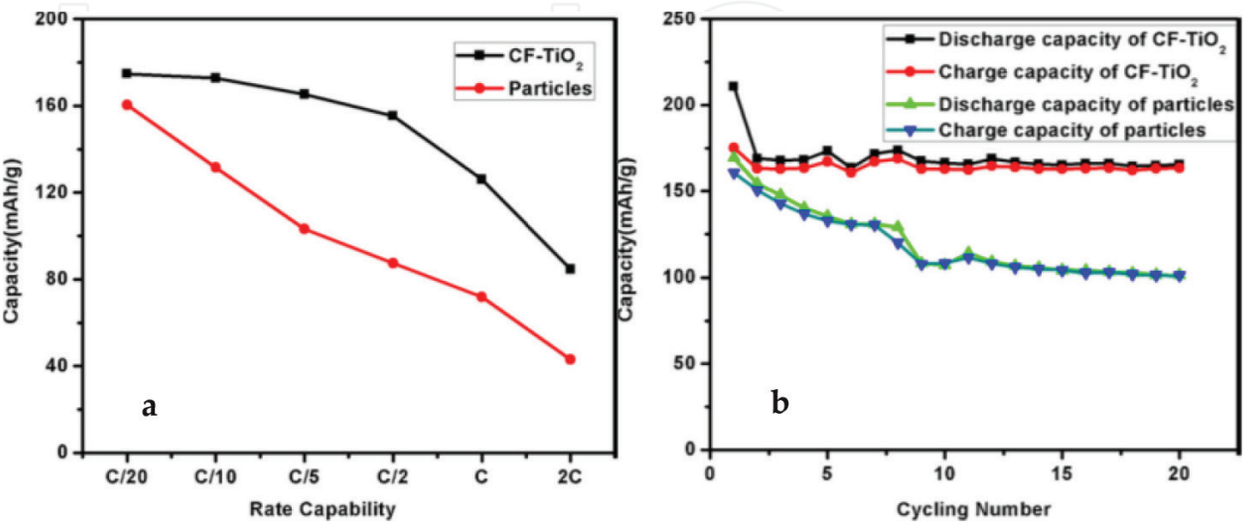

Figure 8. (a) Rate capability and (b) specific discharge capacity comparison of CF-TiO_2 (calcined nanoflakes) and TiO_2 nanoparticles.

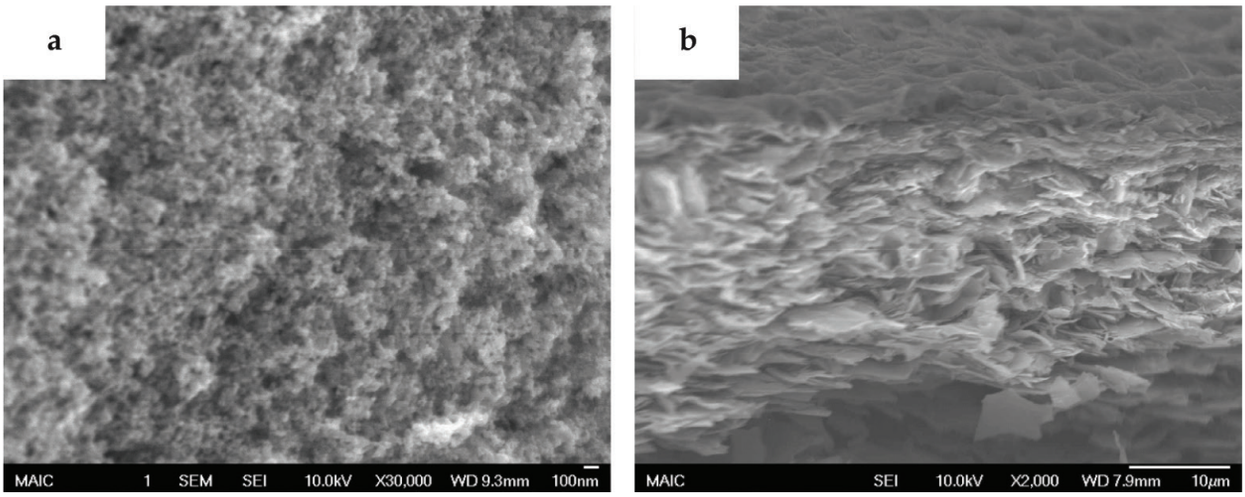

Figure 9. SEM micrographs of sintered photoelectrodes made from (a) P25 nanoparticles (b) calcined titania nanoflakes.

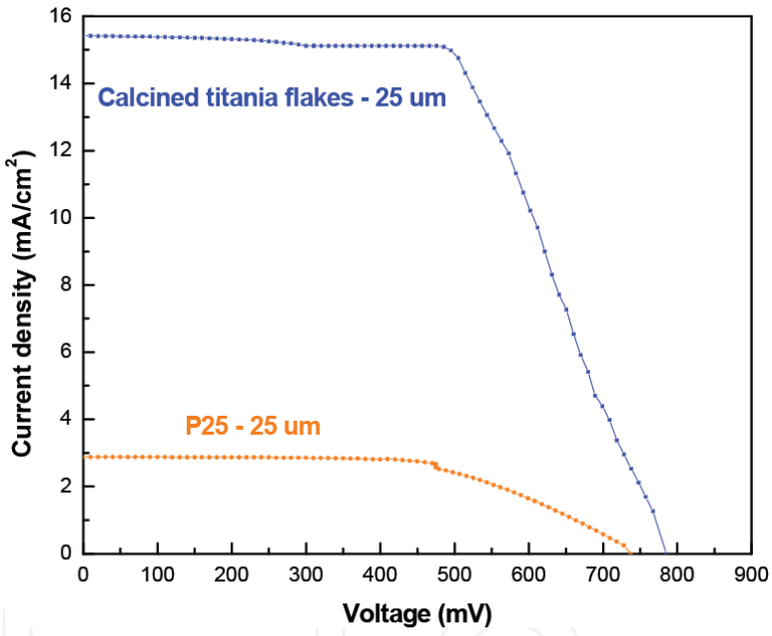

Figure 10. I-V characteristics of DSSCs made from P25 and calcined flakes of similar thickness under AM 1.5 simulated sunlight irradiation.

3. Conclusions

In summary, a high-aspect-ratio titania nanoflakes has been synthesized by the one-step modified surface hydrolysis. Compared to other methods for making low-dimensional nanomaterials, this spreading film process could continuously produce nanoflakes with a cost effective manner. These titania flakes could be easily separated from the treated water by simply sedimentation or filtration and therefore is very suitable for water purification application.

The major summary of applications were listed as follows: (1) Over 99% of methylene blue solution (50 μM) was degraded by the high aspect ratio calcined titania nanoflakes under UVA irradiation within 2 h, whereas not completely decomposition of dye solutions was achieved

using P25 nanoparticles as photocatalysts under the same process condition. (2) Calcined nanoflakes exhibit larger reversible charge/discharge capacity, better rate capability and excellent cycling stability. (3) 7.4% of photon energy conversion efficiency of calcined flakes based DSSC which was 5 times improvement compared to P25 based cell was accomplished.

Acknowledgements

The authors would like to thank Particle Engineering Research Center, University of Florida for support.

Author details

Yang-Yao Lee

Address all correspondence to: yao0708@gmail.com

205 Particle Science and Technology, University of Florida, Gainesville, United States

References

[1] Rothenberger G, Moser J, Gratzel M, Serpone N, Sharma DK. Charge carrier trapping and recombination dynamics in small semiconductor particles. Journal of the American Chemical Society. 1985;**107**:8054-8059

[2] Iijima S. Helical microtubules of graphitic carbon. Nature. 1991;**354**:56-58

[3] Morales AM, Lieber CM. A laser ablation method for the synthesis of crystalline semiconductor nanowires. Science. 1998;**279**:208-211

[4] Pan ZW, Dai ZR, Wang ZL. Nanobelts of semiconducting oxides. Science. 2001;**291**: 1947-1949

[5] Kudo A, Hijii S. H_2 or O_2 evolution from aqueous solutions on layered oxide photocatalysts consisting of Bi^{3+} with $6s^2$ configuration and d^0 transition metal ions. Chemistry Letters. 1999;**28**:1103

[6] Dai ZR, Pan ZW, Wang ZL. Growth and structure evolution of novel tin oxide diskettes. Journal of the American Chemical Society. 2002;**124**:8673-8680

[7] Wang ZL. Zinc oxide nanostructures: Growth, properties and applications. Journal of Physics. Condensed Matter. 2004;**16**:R829-R858

[8] Ye CH, Fang XS, Hao YF, Teng XM, Zhang LD. Zinc oxide nanostructures: Morphology derivation and evolution. The Journal of Physical Chemistry. B. 2005;**109**:19758-19765

[9] Shen GZ, Bando Y, Liu BD, Golberg D, Lee C. Characterization and field-emission properties of vertically aligned ZnO nanonails and nanopencils fabricated by a modified thermal-evaporation process. Advanced Functional Materials. 2006;**16**:410-416

[10] Jang ES, Won JH, Hwang SJ, Choy JH. Fine tuning of the face orientation of ZnO crystals to optimize their photocatalytic activity. Advanced Materials. 2006;**18**:3309-3312

[11] Amano F, Nogami K, Abe R, Ohtani B. Preparation and characterization of bismuth tungstate polycrystalline flake-ball particles for photocatalytic reactions. The Journal of Physical Chemistry C. 2008;**112**:9320-9326

[12] Jang JS, Yu CJ, Choi SH, Ji SM, Kim ES, Lee JS. Topotactic synthesis of mesoporous ZnS and ZnO nanoplates and their photocatalytic activity. Journal of Catalysis. 2008;**254**:144-155

[13] Ye C, Bando Y, Shen G, Golberg D. Thickness-dependent photocatalytic performance of ZnO nanoplatelets. The Journal of Physical Chemistry. B. 2006;**110**:15146-15151

[14] Ying L, Jian D, Peter JH, Meilin L. Synthesis and gas sensing properties of ZnO single crystal flakes. Journal of Materials Chemistry. 2005;**15**:2316-2320

[15] Jinxia D, Xintang H, Hao W, Qiang Z, Fenglou S, Xiang H. Synthesis of porous ZnO micro-flakes via an integrated autoclave and pyrolysis process. Materials Chemistry and Physics. 2007;**106**:181-186

[16] Haibo S, Tianyou P, Ping C, Huabing Y, Chunhua Y. Hydrothermal synthesis of flaky crystallized $La_2Ti_2O_7$ for producing hydrogen from photocatalytic water splitting. Catalysis Letters. 2007;**113**:54-58

[17] Eiji H, Shinobu F, Iraru H, Masaki I, Haoshen Z. Synthesis of the CoOOH fine nanoflake film with the high rate capacitance property. Journal of Power Sources. 2006;**158**:779-783

[18] Pfaff G. Special effect pigments based on silica flakes. Inorganic Materials. 2003;**39**:123-126

[19] Atsunori M, Tatsuo M, Toshihiro K, Kiyoharu T, Tsutomu M, Masahiro T. Formation and characterization of titania nanosheet-precipitated coatings via sol–gel process with hot water treatment under vibration. Chemistry of Materials. 2005;**17**:749-757

[20] Bayykin DV, Friedrich JM, Walsh FC. Protonated titanates and TiO_2 nanostructured materials: Synthesis, properties, and applications. Advanced Materials. 2006;**18**:2807-2824

[21] Peng X, Chen A. Large-scale synthesis and characterization of TiO_2-based nanostructures on Ti substrates. Advanced Functional Materials. 2006;**18**:1355-1362

[22] Liu S, Chen A. Coadsorption of horseradish peroxidase with thionine on TiO_2 nanotubes for biosensing. Langmuir. 2005;**21**:8409-8413

[23] Richter C, Wu Z, Panaitescu E, Wiley RJ, Menton L. Ultra-high-aspect-ratio titania nanotubes. Advanced Materials. 2007;**19**:946-948

[24] Wu JM, Zhang TW, Zeng YW, Hayakawa S, Tsuru K, Osaka A. Large-scale preparation of ordered titania nanorods with enhanced photocatalytic activity. Langmuir. 2005;**21**:6995-7002

[25] Sasaki T, Nakano S, Yamauchi S, Watanabe M. Fabrication of titanium dioxide thin flakes and their porous aggregate. Chemistry of Materials. 1997;**9**:602-608

[26] Moriguchi I, Maeda H, Teraoka Y, Kagawa S. Preparation of a TiO_2 nanoparticulate film using a two-dimensional sol−gel process. Chemistry of Materials. 1997;**9**:1050-1057

[27] Klein LC. Sol-Gel Technology for Thin Films, Fibers, Performs, Electronics and Specialty Shapes. Park Ridge, NJ: Noyes Publication; 1988

[28] Anpo M, Aikawa N, Kubokawa Y, Che M, Louis C, Giamello E. Photoluminescence and photocatalytic activity of highly dispersed titanium oxide anchored onto porous Vycor glass. The Journal of Physical Chemistry. 1985;**89**:5017-5021

[29] Norihito K, Yasuhiko T, Hiroshi H, Junji A, Junji A. Synthesis, characterization, and electrochemical properties of a thin flake titania fabricated from exfoliated nanosheets. Journal of Physics and Chemistry of Solids. 2008;**69**:1447-1449

[30] Li JG, Ishigaki T, Sun X. Anatase, brookite, and rutile nanocrystals via redox reactions under mild hydrothermal conditions: Phase-selective synthesis and physicochemical properties. The Journal of Physical Chemistry C. 2007;**111**:4969-4976

[31] Petr K, Hana L, Olga S, Lenka M, Tomas C. Lamellar micelles-mediated synthesis of nanoscale thick sheets of titania. Materials Letters. 2007;**61**:2931-2934

[32] Shu-Yuan W, Wen-Chi L, Keh-Chang C, Ju-Liang H. Study on the preparation of nano-flaky anatase titania layer and their photovoltaic application. Current Applied Physics. 2010;**10**:S180-S183

[33] Changdeuck B, Hyunjun Y, Sihyeong K, Kyungeun L, Jiyoung K, Myung MS, Hyunjung S. Template-directed synthesis of oxide nanotubes: Fabrication, characterization, and applications. Chemistry of Materials. 2008;**20**:756-767

[34] Bessergenev VG, Pereira RJF, Mateus MC, Khmelinskii IV, Vasconcelos DA, Nicula R, Burkel E, Botelho do Rego AM, Saprykin AI. Study of physical and photocatalytic properties of titanium dioxide thin films prepared from complex precursors by chemical vapour deposition. Thin Solid Films. 2006;**503**:29-39

[35] Yupeng G, Nam-Hee L, Hyo-Jin O, Cho-Rong Y, Kyeong-Soon P, Hee-Gyoun L, Kyung-Sub L, Sun-Jae K. Structure-tunable synthesis of titanate nanotube thin films via a simple hydrothermal process. Nanotechnology. 2007;**18**:295608

[36] Varghese K, Gong D, Paulose M, Grimes CA, Dickey EC. Crystallization and high-temperature structural stability of titanium oxide nanotube arrays. Journal of Materials Research. 2003;**18**:156-165

[37] Almquist CB, Biswas P. Role of synthesis method and particle size of nanostructured TiO_2 on its photoactivity. Journal of Catalysis. 2002;**212**:145-156

[38] Yang-Yao L. Photocatalytic activity and dye-sensitized solar cell performance of high aspect ratio titanium dioxide nanoflakes [Ph.D. dissertation]. Gainesville: University of Florida; November, 2010

[39] Scott B, El-Shall H, Yang-Yao L. A one-step approach to the synthesis of high aspect ratio titania nanoflakes. Global Challenges. 2017;**1**:1700060

[40] Tedeschi S, Stevens N, Cepeda C, Lee YY, Powers K, Ranade M, El-Shall H. Novel supercritical fluid processing techniques for the production of an aerosol. Powder Technology. 2009;**191**:188-193

[41] Fox AM, Dulay MT. Heterogeneous photocatalysis. Chemical Reviews. 1993;**93**:341-357

[42] Hoffmann MR, Martin ST, Choi W, Bahnemann DW. Environmental applications of semiconductor photocatalysis. Chemical Reviews. 1995;**95**:69-96

[43] Hagfeldt A, Gratzel M. Light-induced redox reactions in nanocrystalline systems. Chemical Reviews. 1995;**95**:49-68

[44] Wang YQ, Hu GQ, Duan XF, Sun HL, Xue QK. Microstructure and formation mechanism of titanium dioxide nanotubes. Chemical Physics Letters. 2002;**365**:427-431

[45] Liu AR, Wang SM, Zhao YR, Zheng Z. Low-temperature preparation of nanocrystalline TiO_2 photocatalyst with a very large specific surface area. Materials Chemistry and Physics. 2006;**99**:131-134

[46] Takahashi R, Sato S, Sodesawa T, Arai K, Yabuki M. Effect of diffusion in catalytic dehydration of alcohol over silica–alumina with continuous macropores. Journal of Catalysis. 2005;**229**:24-29

[47] Sasaki T, Watanabe M. Semiconductor nanosheet crystallites of quasi-TiO_2 and their optical properties. The Journal of Physical Chemistry. B. 1997;**101**:10159-10161

[48] Houas A, Lachheb H, Ksibi M, Elaloui E, Guillard C, Herrmann JM. Photocatalytic degradation pathway of methylene blue in water. Applied Catalysis B: Environmental. 2001;**31**:145-157

[49] Ming-Che Y, Yang-Yao L, Bo X, Kevin P, Ying Shirley M. TiO_2 flakes as anode materials for Li-ion-batteries. Journal of Power Sources. 2012;**207**:166-172

[50] Yang-Yao L, El-Shall H. Ultra-high aspect ratio titania nanoflakes for dye-sensitized solar cells. Applied Surface Science. 2017;**426**:1263-1270

IntechOpen